PIPELINE COLLISION AVOIDANCE FOR EXCAVATION WORK USING MAGNETIC ANOMALY DETECTION (MAD)

A Thesis

by

CAMERYN SUMMER LOPEZ

Submitted to the Graduate and Professional School of
Texas A&M University
in partial fulfillment of the requirements for the degree of

MASTER OF SCIENCE

Chair of Committee,	Jeonghee Kim
Co-Chair of Committee,	Ana Goulart
Committee Member,	Youngjib Ham
Head of Department,	Reza Langari

May 2022

Major Subject: Engineering Technology

ABSTRACT

Uncertainty of the precise location of underground pipelines poses a safety risk to excavator operators and nearby construction workers. Excavator collisions with pipeline carrying hazardous material can result in significant injuries or fatalities along with increased project time for repair. The current methods for warning operators of nearby pipelines only provide the approximate location. There is then a need for locating the pipeline in real-time and properly alerting excavation operators of the proximity of the machine to a pipeline. Several methods have been implemented for underground object detection: ground penetrating radar (GPR), electromagnetic signal generation, acoustic excitation, and magnetic anomaly detection (MAD). Among these methods, MAD has been found to be the most suitable for the case of a moving sensor and stationary ferromagnetic target. MAD exploits the magnetic anomaly created by large ferromagnetic material to locate underground structures. A magnetic anomaly is detected when the measured geomagnetic field deviates from its expected value at a particular point. Current magnetic anomaly inversion techniques are complex and time-consuming, and thus implementation at excavation jobsites is not practical. The work described in this paper utilizes two magnetometers to cancel the geomagnetic background and effectively estimate the proximity to a steel pipeline in real-time.

ACKNOWLEDGEMENTS

I am deeply grateful to my committee chair, Dr. Kim, for her invaluable guidance, encouragement, and patience during my study. I would also like to thank my committee members Dr. Goulart and Dr. Ham for their time and support throughout the course of this research.

I would like to acknowledge the efforts and special contribution put forth by the Earth Vision team in developing the multi-node sensor system that was employed in this project. Thanks also to my colleagues Bing, Jeongjae, Travis, Leon and Bernard for their feedback and for fostering a great team environment.

Finally, I would like to extend my appreciation to my parents for their love and support throughout my years of schooling.

CONTRIBUTORS AND FUNDING SOURCES

Contributors

This work was overseen by a thesis committee consisting of Dr. Jeonghee Kim and Dr. Ana Goulart of the Department of Electronic Systems Engineering Technology and Dr. Youngjib Ham of the Department of Construction Science. The wireless multi-node sensor system described in Section 3 was designed and fabricated by the senior design team, Earth Vision (2021). All other work conducted for the thesis was completed by the student independently.

Funding Sources

Graduate study was supported by a graduate assistantship provided by the Department of Engineering Technology and Industrial Distribution at Texas A&M University. This work was also made possible in part by NSF under Award Number 2026574. Its contents are solely the responsibility of the authors and do not necessarily represent the official views of the NSF.

TABLE OF CONTENTS

Page

LIST OF FIGURES

Page

LIST OF TABLES

Page

1. INTRODUCTION

1.1. Background

The uncertainty of the precise location of buried infrastructure presents a challenge to excavator operators and nearby construction workers. While workers are trained and primed to follow numerous safety measures, pipeline incidents due to excavation damage continue to pose a serious safety risk. From 2017 to 2021, pipeline incidents due to excavation damage were responsible for 20% of the injuries and 30% of the fatalities in all reported pipeline incidents in the U.S. [1]. The ramifications of such an incident are detrimental, including significant costs for repairment, environmental damages, and loss of essential services. Prior to digging, project managers are required to call 811 to request that the area be surveyed and marked with flags to indicate the approximate location of underground pipelines. Despite having this information, the exact location of the pipeline remains ambiguous during the excavation process.

Providing information about the location of a buried pipeline and its distance from heavy machinery in real-time will minimize construction accidents due to pipeline collision and the resulting damage to critical infrastructure. Simple proximity information enables excavator operators to promptly become aware of the situation while location details issued from utility companies may be overwhelming and not always reliable. The burden and uncertainty of information can be particularly daunting in dynamic environments such as construction sites. This research creates an avenue for reducing the job stress that arises from this uncertainty and subsequently promotes the improvement of workplace safety in the construction industry.

1.2. Pipeline Detection Methods

The use of technology such as monitoring systems and detection systems have been suggested to improve the pipeline locating process [2]. While several hand-held devices such as magnetic locators, pipeline locators and cable avoidance tools (CAT) can be used prior to digging, the technology is unable to predict the exact distance to buried pipeline during an ongoing excavation event. Nevertheless, the technology used in commercially available pipeline locators should be studied for potential applicability to the excavation scenario. In general, two approaches have been investigated: The first involves active signal transmission through the ground area of interest, where detection is dictated by the refracted signal. The second is a passive approach, utilizing the characteristics of the measured interference. This section will present a review of the methods explored in literature that are guided by these approaches.

1.2.1. Ground Penetrating Radar

Among the techniques for locating underground pipelines through signal transmission, there is wide research interest in utilizing different forms of ground penetrating radar (GPR) to detect both metallic and non-metallic material. GPR technology employs a generator to source an electromagnetic signal, a transmitter to cast the waves outward, and a receiver to capture the reflected waveforms coming from objects in the transmission path. Different radar system frameworks have been used for radar generation, including impulse radar, chaotic signal radar, and ultra-wideband radar. Ultra-wideband (UWB) radar is an emerging research area because it provides strong penetration and good range resolution [3]. Li et al introduced a system of UWB chaotic signals in pipe detection, proposing a range resolution of 10 cm [4].

Nevertheless, detecting underground objects with GPR is difficult due to the variation of the dielectric properties as the wave passes through different media underground [5-6]. Careful interpretation of the reflected signal is thus significant in distinguishing buried objects and determining their depth and position. Characteristics of the buried object are recognized through their signature in radar images, and cylinder-shaped objects such as pipelines are revealed as hyperbolic signatures [7]. Hyperbolic fitting techniques have then been examined for pipeline position [8-10] and orientation estimation [11]. Conductive materials in the media also compromise the effectiveness of GPR, causing the waveform to attenuate and thus face weaker penetration. Though filtering methods have been proposed to improve GPR detection and localization accuracy [12], the prospect of mounting a GPR system to an excavator introduces additional complexities.

1.2.2. Acoustic Transmission

In a similar fashion to the GPR method, the acoustic method uses the propagation characteristics of sound waves to localize buried utilities. This method can either be carried out through excitation of the pipe or of the ground, however, pipe excitation requires access to the pipeline. Excitation of the ground can be accomplished through seismic waves or point vibration measurements. Zahari et al used the seismic reflection technique with compressional wave propagation to detect and characterize buried objects [13]. While this method allows for the detection and identification of the pipe with 88% accuracy, there still exists a need for real time data collection. Another acoustic positioning method described by Dai and Xu exploits the good time domain composition and frequency domain characteristics of the Golay sequence as the

transmission signal and can achieve up to 92% detection accuracy [14]. However, this method is not suitable for cases where the target or measurement device is in motion.

1.2.3. Electromagnetic Localization

The active implementation of the electromagnetic localization method involves using a transmitter to generate electromagnetic waves that are directed toward the area of interest and a receiver that detects any resulting induced electric field. The only active transmission technique that doesn't require direct access to the pipeline is the induction method. Some researchers have used pulse induction electromagnetic coils to scan the soil during an excavation event. [15-16] The technology operates on the eddy current principle whereby eddy currents into conductive material can be induced and detected by the process of applying and subsequently removing current from the sensor coil. While this method can produce reliable information about the pipe location, the scanning process is lengthy and thus cannot provide real-time feedback to the operator as the excavation takes place.

The passive implementation of electromagnetic localization already used in commercially available products relies on detecting electric field from cables that are already carrying current. Other factors that contribute to the reliability of electromagnetic localization include frequency range, transmitter placement, soil conditions, and the method only applies to locating metallic structure. To avoid these issues, it is suggested that magnetic anomaly detection (MAD) be used as a passive technique that is not critically impacted by such factors.

1.2.4. Magnetic Anomaly Detection

For ferromagnetic targets, where either the target or measurement device is in motion, magnetic anomaly detection has been shown to be effective in real time [17]. MAD exploits the magnetic anomaly created by large ferromagnetic material to locate underground structures. A magnetic anomaly is detected when the measured geomagnetic field deviates from its expected value at a particular point. Thus, the field generated by the anomaly can be captured as follows,

$\overrightarrow{B_a} = \overrightarrow{B_m} - \overrightarrow{B_e}$

where $\overrightarrow{B_m}$ is the measured field and $\overrightarrow{B_e}$ is the expected field. MAD has been long-established within the defense and intelligence community for detecting submerged enemy submarines. In this case, magnetic anomaly detection units are commonly mounted to aircrafts to survey the area, and the target can be treated as a magnetic dipole point source as a result of the large distance between the target and the sensor [18]. Research in this area has presented an orthonormalization method to deal with the complexity of a moving target or moving sensor. Using the orthonormalization method, the measured field under the assumption of a dipole target can be broken down into a set of orthonormal basis functions (OBFs) [19-20]. However, ferromagnetic pipelines cannot be approximated with a single dipole structure when the pipeline is close to the sensor, as in the case of mounted MAD systems on excavator equipment. The method must then be adapted to consider a number of dipole elements along an infinite pipeline. Magnetic dipole reconstruction method (MDRM) can be applied to geometrically simulate the magnetic intensity of underground ferromagnetic pipelines. The notion of MDRM involves breaking up the pipeline into a finite number of magnetized elements that each contribute a magnetic intensity and then summing the intensities to achieve an overall magnetic intensity of the observed area.

Sheinker and Moldwin approximated the magnetic field of an infinite pipeline with an array of N dipole elements, each having a magnetic moment, m. The researchers created an effective magnetic anomaly detector using principal component analysis (PCA) on simulated magnetic fields produced through various configurations of the following variables: pipeline orientation, geomagnetic field, and magnetic moment and orientation contributed by each dipole element. To eliminate the presence of various noise influences, two of the principal components were used to form matched filters. The matched filters correlate the measured signal with the principal components to extract the actual field signal. Then, detection of the anomaly is achieved by observing the energy index obtained from the squared sum of the filtered signals [21]. Magnetic dipole reconstruction (MDR) method has been useful in determining pipeline geometry such as straight sections, bends and elbows, and tee joints [22].

While numerous studies have employed MAD to detect buried objects, only several have implemented magnetic anomaly inversion for pipeline localization. To avoid large construction vehicles from colliding with buried pipeline, the precise location of the pipeline should be determined. Different segmentation techniques used in MDR impact the accuracy in the inversion process. MDR for magnetic anomaly inversion has been shown to achieve high accuracy in simulation, but it suffers from long computation time [23-24]. The approach described in [25] is used to measure the depth of a buried steel pipeline when two measurements are taken laterally to the pipe centerline using an array of three-axis magnetometers. Another inversion method calculates the burial depth of pipeline by using the AM-PSO algorithm on synthetic magnetic strength data for iron pipeline [26].

Interference from nearby magnetic sources must be greatly reduced. MAD research interest is largely focused on developing algorithms that compare sensor data with a reference

sensor to filter out background noise. One novel method presented by Chen et al suggests fusing magnetic field data from sensor arrays using signal modulation to further improve detection accuracy [27].

1.3. Magnetic Field Characteristics of Ferromagnetic Pipeline

There are a handful of challenges imposed when assessing the magnetic field characteristics of ferromagnetic pipelines. Historical uses for MAD involve treating the target as a magnetic dipole point source, but this is not realizable with long structures as the distance between the pipe and measurement device must be 3 times the size of the target [21] to reduce the structure to a point source. It has then been suggested to view the pipeline as an array of dipoles with the magnetic field contributed by a single element is given by,

$$B_n = \frac{\mu_0}{4\pi}\left[\frac{3(m*r_n)r_n}{{r_n}^5} - \frac{m}{{r_n}^3}\right]$$

Then the approximate magnetic field of the pipeline is given by the net sum of all the individual dipole elements. This approximation requires the target to be sufficiently far from the measuring device to neglect local anomalies. For pipeline detection at construction sites, this approximation is not feasible. The present work focuses on an 18-in pipeline section. The magnetic field of this section was characterized by taking magnetic field strength measurements along the length of the pipeline. The midpoint of the pipeline section can be indicated by a change in polarity or minimum while the endpoint of the pipeline section can be identified through maximum magnitude [25].

2. ESTIMATING DISTANCE TO A FERROMAGNETIC PIPE SECTION

2.1. Method

Known characteristics of a ferromagnetic pipeline section gathered through experimental data collection can be utilized to formulate mathematical models describing the relationship between magnetic field strength and distance. Two wireless sensor modules, denoted by *mag* and *ref*, respectively, were used to implement MAD. One module was used to measure the magnetic field close to the pipeline and the other was used as a reference to capture the local magnetic field. To expose the anomalous field created by the pipeline section, the magnetic field strength measured by the reference module was subtracted from the module closest to the target. The three-axis anomalous fields, B_{ax}, B_{ay}, and B_{az}, were captured as follows,

$$\begin{aligned} B_{ax} &= B_{x,mag} - B_{x,ref} \\ B_{ay} &= B_{y,mag} - B_{y,ref} \\ B_{az} &= B_{z,mag} - B_{z,ref} \end{aligned} \tag{1}$$

The total magnetic anomaly, B_{aT}, is then the square of the horizontal and vertical components,

$$B_{aT} = \sqrt{(B_{ax})^2 + (B_{ay})^2 + (B_{az})^2} \tag{2}$$

Using the described method and measuring along the length of the pipe, the total magnetic anomaly of a steel pipe section is revealed and shown in Figure 1.

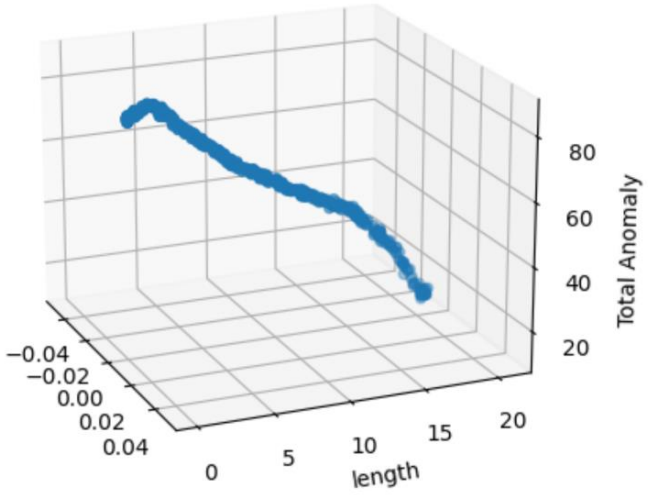

Figure 1. Magnetic Field Strength of a Steel Pipe

2.2. Preliminary Experimental Setup

Magnetic field data was collected from an A500 structural steel pipe with a 5-in outer diameter against the geomagnetic background by the measurement apparatus. The apparatus consisted of two BNO055 Inertial Measurement Units (IMUs) and an HC-SR04 ultrasonic sensor mounted on a foldable wooden ruler with data transmitting to an Arduino Nano. The first IMU was mounted at the front end of the ruler and the second IMU was spaced 2 ft from the first, both oriented with x-axis parallel to the ruler. The IMUs can be denoted by *mag* and *ref*, respectively. Data was transmitted using I^2C via wired connections running from the sensors to the Arduino Nano. The sensor data was sent to a laptop for acquisition and processing. The purpose of the ultrasonic sensor was to provide reference distance measurements. It was placed 5 inches from the front end of the ruler to reduce possibilities for interference with mag. The experimental setup is shown in Figure 2.

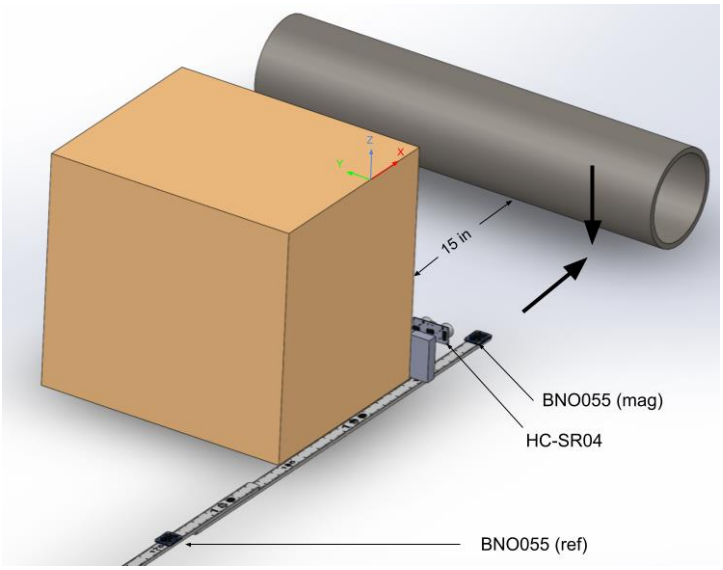

Figure 2. Preliminary Experimental Setup

The apparatus was first used to measure the magnetic field strength along the length of the pipeline to determine a useful point of interest. It was decided that the end of the pipe, where the magnetic field strength was the greatest, would be the focus point for the following tests. Magnetometer readings were taken from both IMUs as the apparatus was pushed towards the pipe. To eliminate the local magnetic field, the magnetic field strength measured by the reference IMU (ref) was subtracted from the IMU closest to the pipe (mag). Data was collected for two motion scenarios: horizontal and vertical motion. To isolate motion along the x-axis, the ruler was guided along the side of a cardboard box. A similar arrangement was made to isolate motion along the z-axis when assessing the vertical anomaly. During both motion scenarios, the x-axis of the BNO055 was aligned with magnetic north, and the pipe section was placed perpendicular to it, as shown in Figure 2. It was important to fix the orientation of the pipe section with respect to magnetic north to maintain consistent measurements. Measuring from different angles would result in a different magnetic field vector, thus changing the characteristic curve from trial-to-

trial. The ultrasonic sensor was used to measure the actual distance from the front IMU to the pipe in both scenarios.

2.2.1. Horizontal Motion Testing

The horizontal motion test consisted of sliding the ruler 10 inches to the endpoint of the pipe while magnetometer data was collected and recorded. The magnetic field strength was captured for all three axes, along with the total magnitude. This test was also completed without the pipe present to determine the effect of motion on the recording, if any. The horizontal magnetic anomaly field strength, B_x, grew exponentially as the apparatus approached the focus point. This relationship was also represented in the total magnitude of the anomaly, B_T, including both horizontal and vertical field strength components. It can then be concluded that the measured anomaly along the axis of motion contributed the most to the total, thus it may be a good metric of interest for distance estimation. These relationships, compared against the geomagnetic background, are shown in Figure 3.

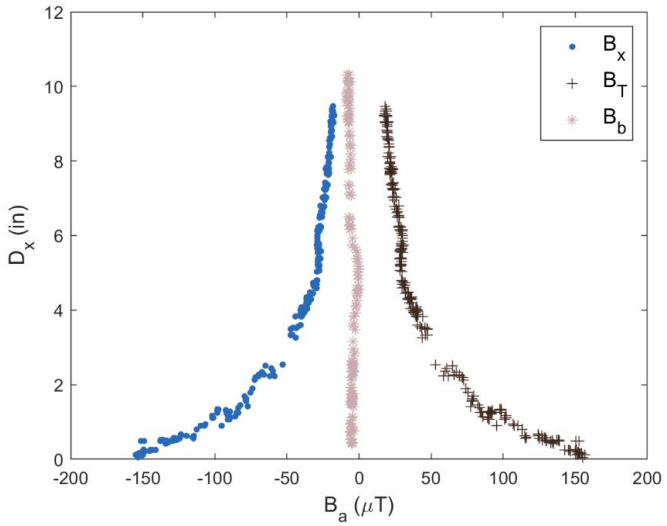

Figure 3. Horizontal Anomaly Characteristic of Target

2.2.2. Vertical Motion Testing

A model for the vertical anomaly was also determined in a similar fashion. The apparatus was held 10 inches above the focus point and then lowered by sliding the ruler down a box. Figure 4 shows the vertical anomaly. For distances greater than 4 inches from the pipe, the vertical and total magnitude closely follow each other, demonstrating an expected inverse-square relationship. Like the horizontal motion testing scenario, this result also suggests that the anomaly along the axis of motion is the strongest. However, as the sensor moves closer to the pipe, there is some variation.

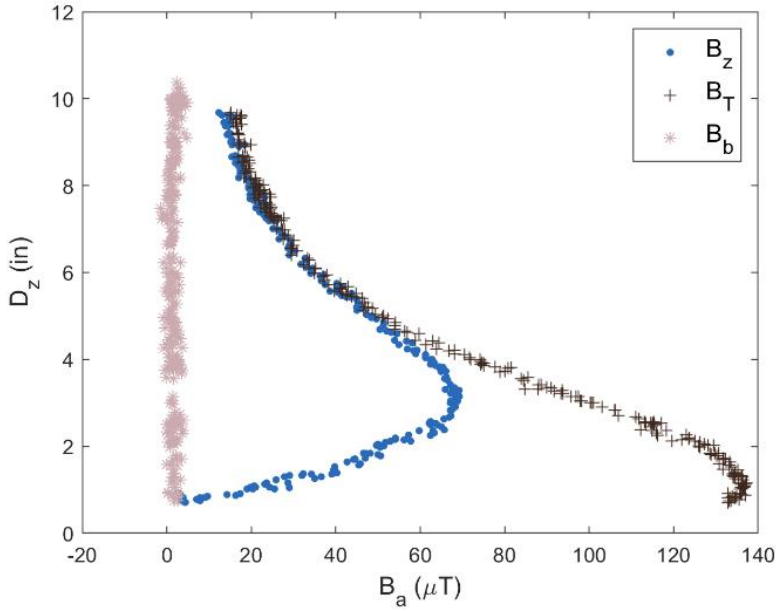

Figure 4. Vertical Anomaly Characteristic of Target

2.3. Distance Estimation Results

The estimated distance as assessed through the proximity models was compared with the actual distance measured by the ultrasonic sensor. This comparison result is shown in Figure 5. Distance estimation using the horizontal proximity model was found to be a good indicator of the actual distance from the pipe throughout the total distance. In this trial, the vertical proximity model was able to accurately estimate the distances between 3.5 and 6.5 in, but distances close to the pipe were not able to be estimated using this model.

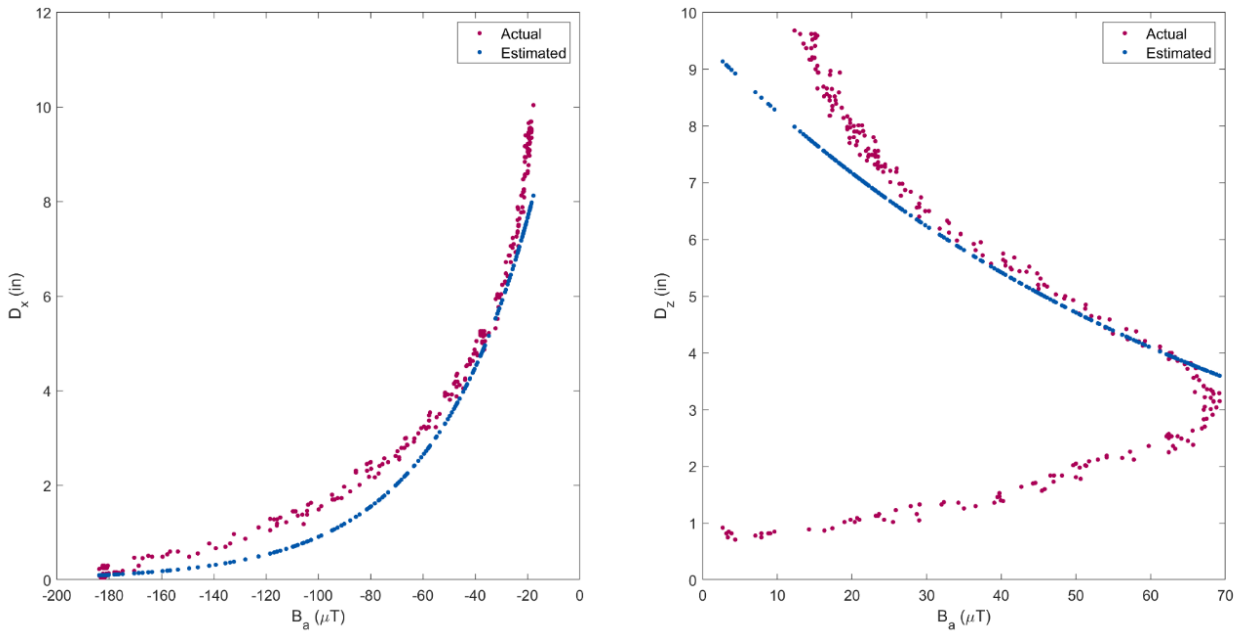

Figure 5. Horizontal and Vertical Distance Estimation

Distance estimation using the horizontal anomaly model had higher accuracy for distances between 4 and 8 inches and some deviation for distances lower than 3 inches. The following tables break down the errors associated with different distance regions. The high error

reflected in Table 2 indicates that further processing for distances close to the pipe is needed to accurately estimate the distance. Improvement of this accuracy is presented in Section 3.

Table 1. Horizontal Distance Estimation Error

	BNO055	
Range (in)	Error (%)	Std
9 – 6	11.8	4.83
6 – 3	8.40	4.92
3 - 0	38.0	13.2

Table 2. Vertical Distance Estimation Error

	BNO055	
Range (in)	Error (%)	Std
9 – 6	9.80	3.82
6 – 3	4.39	4.02
3 – 0	296	327

It should be expected that the magnetometer readings from trial-to-trial stay consistent since they are taken from the same point on the pipeline. The extreme deviation in readings when the apparatus is very close to the pipe could be attributed to the magnetometer becoming magnetized by the strong field created by the pipe. Further, if the electrical currents in the IMU are varying, this would result in subsequent varying magnetic field lines. While arrangements

were made to isolate motion along the x-axis, other variations in accuracy can be attributed to small deviations from the movement path, along with inconsistent speed across trials. These inconsistencies would have a greater effect at smaller distances due to the increased density of field lines very near the pipe.

In general, the experiment in section 2 confirms the feasibility of performing distance estimation using two moving magnetometers. This experiment focused on exploiting the horizontal and vertical anomalies produced by a steel pipe in the presence of the surrounding geomagnetic field. It is shown that the representative models are not significantly affected by acceleration, thereby confirming the utility of magnetometers in a construction scenario. The simple magnetic field subtraction also allows the proximity estimate to be calculated quickly, thus it would be good for a real-time application.

Though the experimental results represent isolated horizontal and vertical motion, the full range of excavator motion is not represented. These experiments also involved stable movement, but the magnetometer readings may be impacted by the vibrations and random movements of the excavator. A real-world implementation of this system will need to be wireless to allow for flexibility in sensor placement and data aquation. Further processing on the magnetic anomaly signal will also be required to reduce the error.

3. REAL-TIME DISTANCE ESTIMATION SYSTEM

In section 2, the efficacy of developing proximity models through motion isolation using off-the-shelf sensors and a preliminary experimental setup was shown. In this section, the development of a real-time wireless system for proximity estimation is provided, and the method for estimating the distance of a pipeline from a moving model excavator will be described and evaluated. Along with the BNO055, a second sensor is introduced in the system for redundancy when testing the method. The performance results of the sensors will also be compared. An overview of the real-time proximity estimation system is illustrated in Figure 6.

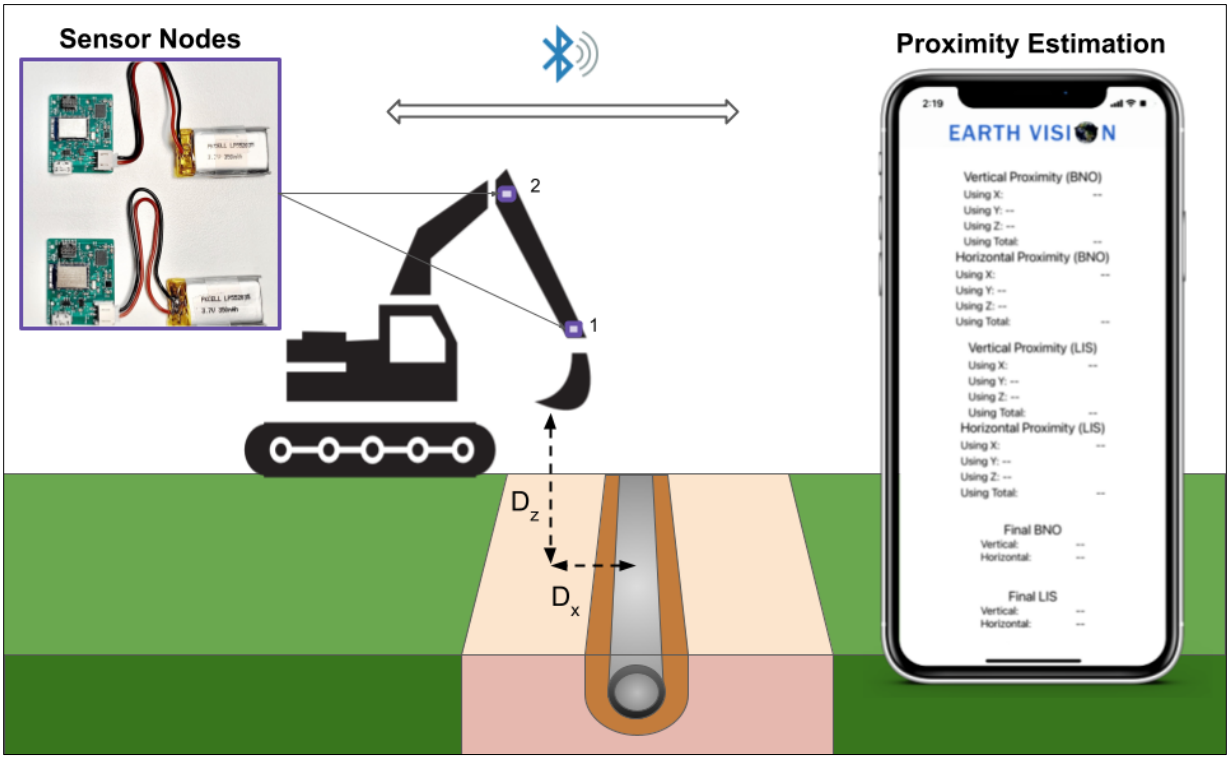

Figure 6. Real Time Distance Estimation System

3.1. Wireless Multi-Node Sensor System

3.1.1. Hardware

The custom wireless system shown in Figure 7 was designed and fabricated by Earth Vision. The system hardware consists of PCB modules that collect and send data over Bluetooth to a custom iOS application. Each module includes a BNO-055 inertial measurement unit (IMU), LIS3MDL triple axis magnetometer, Raytac MDBT42Q system on chip, and a lithium-ion battery charger. The system block diagram is shown in Figure 8. The compact, 2 square-inch design of each module enables flexibility when determining the best locations for mounting the system on the excavator. Each node can be powered with a 3.7V lithium-ion battery. The PCB also has a built-in battery charger, in which a USB to micro-USB connector can be connected from the device to a 5V power source to charge the lithium-ion battery.

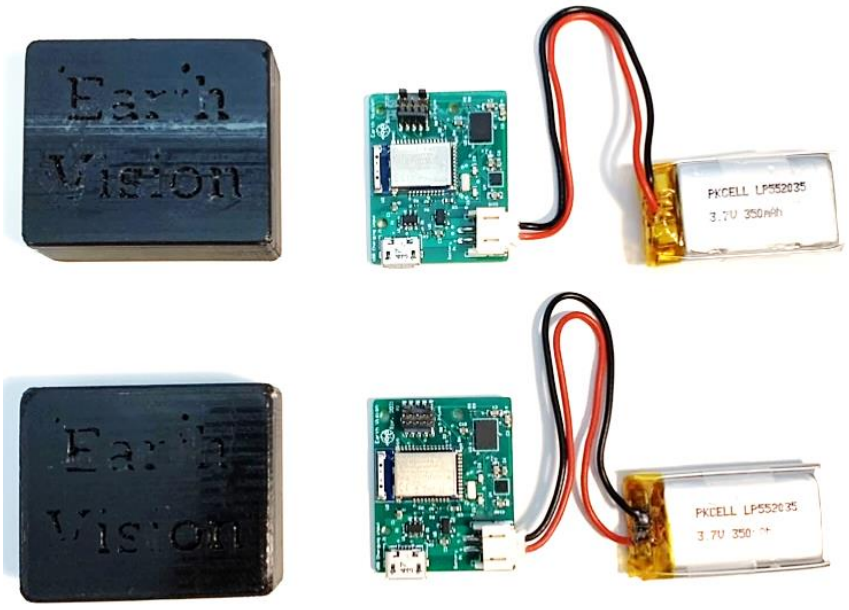

Figure 7. Earth Vision Wireless Sensor Modules and Hardware Enclosure

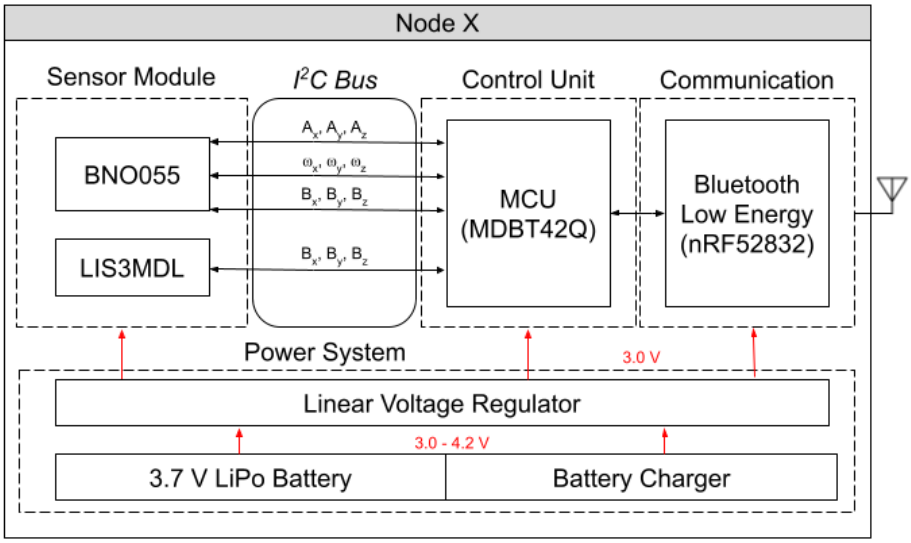

Figure 8. Earth Vision Sensor Module Block Diagram

The BNO-055 System in Package (SiP) was included in the sensor modules to offer a solution for pinpointing the location, orientation, and acceleration of a particular module while data is remotely collected. The IMU provides 9 degrees of freedom, measuring triaxial accelerometer, gyroscope, and magnetometer data. As a Bosch product, the sensor is equipped with 32-bit microcontroller intelligence and internal algorithms that can be activated for sensor calibration and filtering. The magnetometer typically offers 0.3 µT resolution and magnetic field range of ±1300 µT for the x and y axes and ±2500 µT for the z axis.

The LIS3MDL is a digital output three-axis magnetic sensor with 16-bit data resolution. The sensor has user-selectable full-scale ranges of ±4/±8/±12/±16 gauss and wide supply voltage range from 1.9 V to 3.6 V. By default, the lowest range of ±4 gauss or 400 µT is used in the sensor module. The sensor specifications for the LIS3MDL and BNO055 are summarized in Table 3.

Table 3. Sensor Specifications adapted from [28] and [29]

BNO055		
Specification	Value	Unit
Magnetic field range	±1300 (x-, y-axis); ±2500 (z-axis)	µT
Magnetic field resolution	~0.3	µT
Gain error	±5	%
Sensitivity temperature drift	0.01	%/K
Zero-B offset	±40	µT
LIS3MDL		
Measurement range	±400	µT
Magnetic field resolution	~0.015	µT
Zero-gauss level	±100	µT

The Raytac MDBT42Q is the chip antenna module designed for the Nordic nRF52832 solution. It features a 32-bit ARM Cortex – M4 CPU, full set of digital interfaces, DC/DC buck converter, and it supports Bluetooth Low Energy (BLE). The LIS3MDL and BNO055 communicate with the controller unit via an I^2C serial bus, and the sensor data is transmitted through Bluetooth to a mobile device.

A custom iOS application was designed to capture and display the transmitted sensor data. The user can connect and disconnect individual sensor nodes from the central Bluetooth node and view real-time sensor measurements through the application. The iOS application was further developed to provide information about the estimated distance between the pipe section and the excavator. Serving as an aid for data collection and analysis, the application was designed to calculate the anomalous field along each axis, apply the relevant linear model, display the result in real-time, and then save all collected data to a .csv file for further analysis. The sensor data can be collected and displayed in the application at a rate of 5 Hz.

3.1.2. Software

The system software relies on BLE connections between a central node and two peripheral nodes. The peripheral nodes consist of the individual sensor modules containing node-specific firmware. Each node was programmed to collect sensor data and connect to the central node using BLE. The software flowchart for a peripheral node is shown in Figure 9. In this paradigm, the sensors are first initialized at the default setting. The Bluetooth module is then configured and begins advertising. Once the peripheral node has been discovered by the central node, the sensor data is read and then posted.

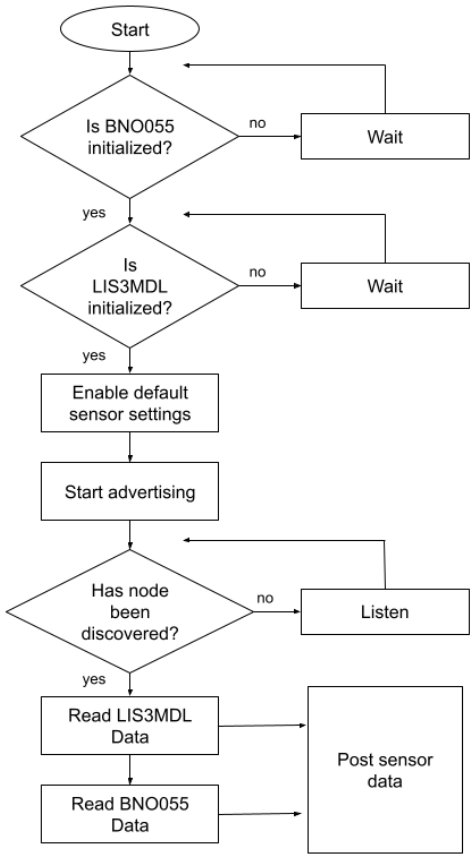

Figure 9. Peripheral Node Software Flowchart

The mobile device running the IOS application functions as the central node. The software flowchart is provided in Figure 10. First, Bluetooth is initialized and the device scans for available advertisements. If a peripheral node is discovered on the same advertising channel, the central node can request a connection. Once the connection is created, the central node can begin to receive the data transmitted from the sensor module. The data received is then processed by the proximity estimation algorithm described in the following section.

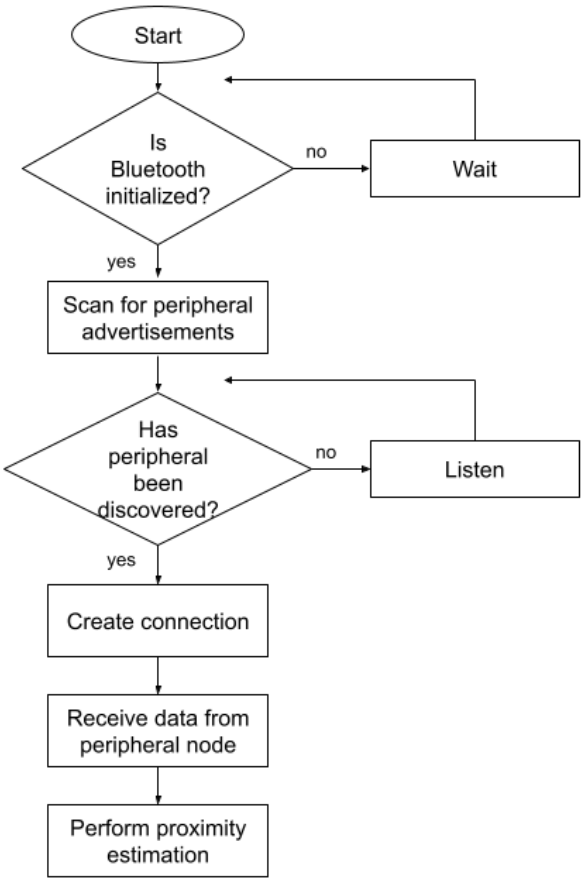

Figure 10. Central Node Software Flowchart

3.2. Experimental Setup

3.2.1. Horizontal Motion Testing

The experimental setup for horizontal motion is shown in Figure 11. In the horizontal motion scenario, the excavator boom and arm are not actuated, and the excavator is simply driven forward over the buried pipeline section and perpendicular to the longitudinal axis of the pipe. The excavation construction scenario was emulated using a TR-211 remote control excavator and an A500 structural steel pipe.

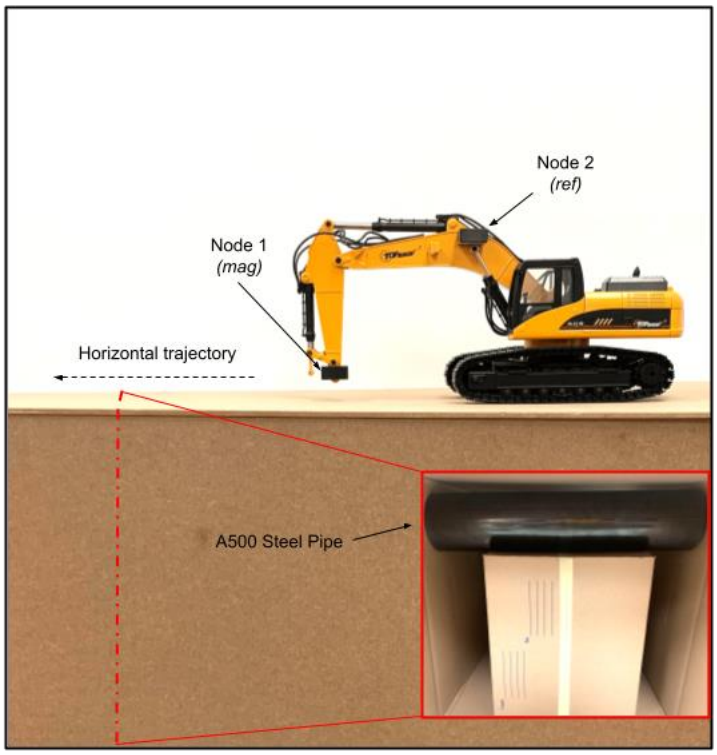

Figure 11. Experimental Setup for Horizontal Motion Tests

To model a horizontal scanning scenario, the excavator was driven along a 30-in box, passing the pipe section located in the inside of the box. This cross-section is indicated in red.

The measured distance between the outer diameter of the pipe section and the first sensor module was 1.25 in, and the distance between the sensor modules was 12 in. An ultrasonic sensor was mounted to the front of the arm to measure the distance of the first module with respect to the pipeline. The excavator was driven towards the target at full speed by pressing the left and right joysticks of the controller forward. Though the excavator motion was directed perpendicular to the length of the pipe section, the excavator tended to drift slightly from the straight-line path on either side. While the excavator was in motion, the sensor modules measured the anomalous magnetic field and transmitted this data to an iPhone XR. Data for this scenario was collected through three different runs to capture slight deviations from the intended path.

The anomalous field strength along each axis as measured by the BNO055 and LIS3MDL sensors is shown in Figure 12. Horizontal distance from the centerline of the pipe section was measured in inches. Positive distance values indicate the excavator was moving toward the target while negative distance values indicate that the excavator has crossed the pipe section and was moving away from the pipe. Across all runs, there was an apparent inflection point at the 0-inch mark which corresponds to a point directly over the outer diameter of the pipe section. This result is consistent with the magnetic field of a bar magnet, whereby the magnetic field lines at the poles of the magnet on either side are opposing.

The measured magnetic field anomaly along the x-axis when aligned with magnetic North thus can provide information about the position of the sensor relative to the pipeline. It is also shown that the magnetic field strength can be related linearly to distance for distances less than 10 in.

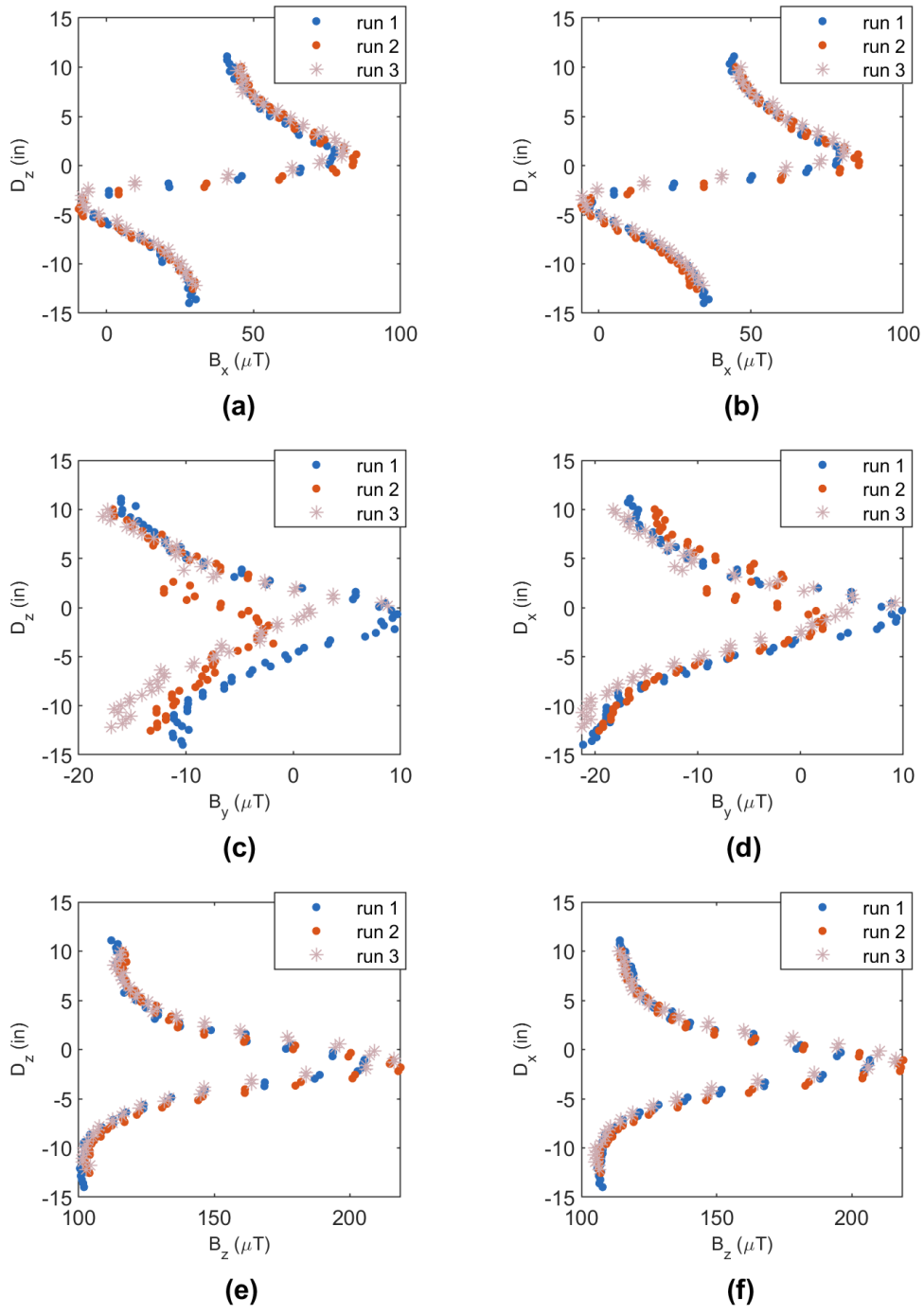

Figure 12. 3-DOF Raw Magnetic Anomaly Data as Measured by BNO055 and LIS3MDL in Horizonal Motion Testing. (a), (c), (e) Magnetic anomaly measured by BNO055 in X, Y, and Z axes, respectively. (b), (d), (f) Magnetic anomaly measured by LIS3MDL in X, Y, and Z axes, respectively.

The average of the three runs for each sensor is shown in Figure 13. This result was used to generate the following proximity models,

$$D_x(B_{ax}, B_{aT}) = \begin{cases} -0.2441B_{ax} + 19.67 & if \quad 40 < B_{ax} < 100\ \mu\text{T} \quad (3) \\ -0.2073B_{ax} - 5.63 & if \quad -10 < B_{ax} < 40\ \mu\text{T} \quad (4) \\ -0.0707B_{aT} + 13.72 & otherwise \quad (5) \end{cases}$$

where (3) and (4) provide the proximity of the excavator when it is respectively approaching and then leaving the target. Distances 2 inches from the pipeline is given by (5).

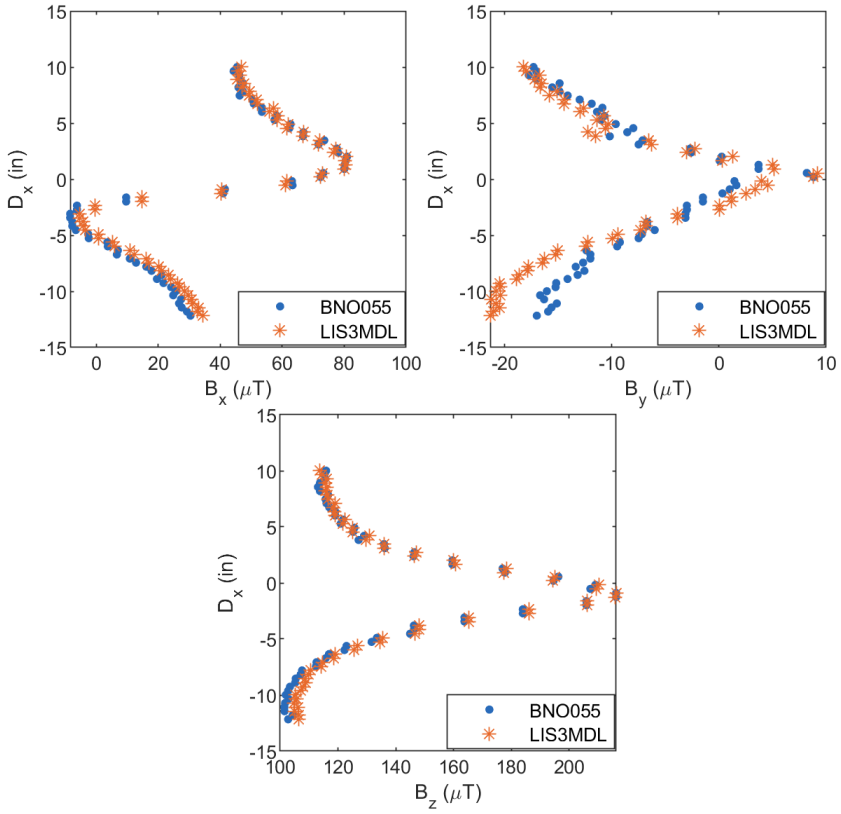

Figure 13. Average 3-DOF Magnetic Anomaly in Horizontal Motion Testing

The algorithm shown in Figure 14 was developed to reflect the sensor position relative to the pipeline in the real-time system. The algorithm utilizes the different magnetic field strength ranges measured while the sensor is in motion. Since the anomaly measured along the x-axis consists of distinct ranges that correspond to either side of the pipe, the algorithm first checks whether the excavator is approaching or leaving the pipeline. The respective linear models are then applied to estimate the distance. At around 2 inches, these models begin to produce inaccurate results, thus the total anomaly model is used to calculate distances very close to the pipe.

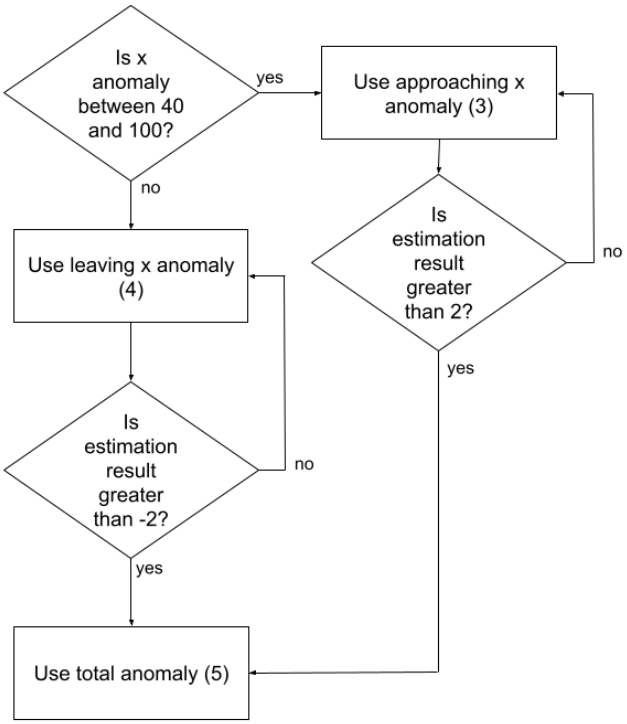

Figure 14. Horizontal Position Estimation Algorithm

3.2.2. Vertical Motion Testing

In the vertical motion scenario, illustrated in Figure 15, only the excavator boom is actuated such that the tip of the arm moves down toward the pipe section. The starting position of the *mag* sensor module was 12 in from the pipe. Magnetic field strength information was recorded for three trials. The anomalous field strength along each axis as measured by the BNO055 and LIS3MDL sensors is shown in Figure 16.

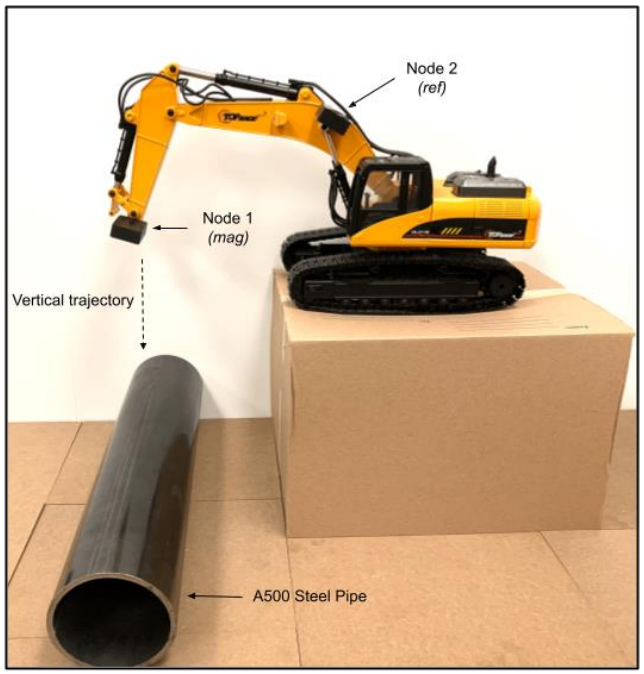

Figure 15. Experimental Setup for Vertical Motion Tests

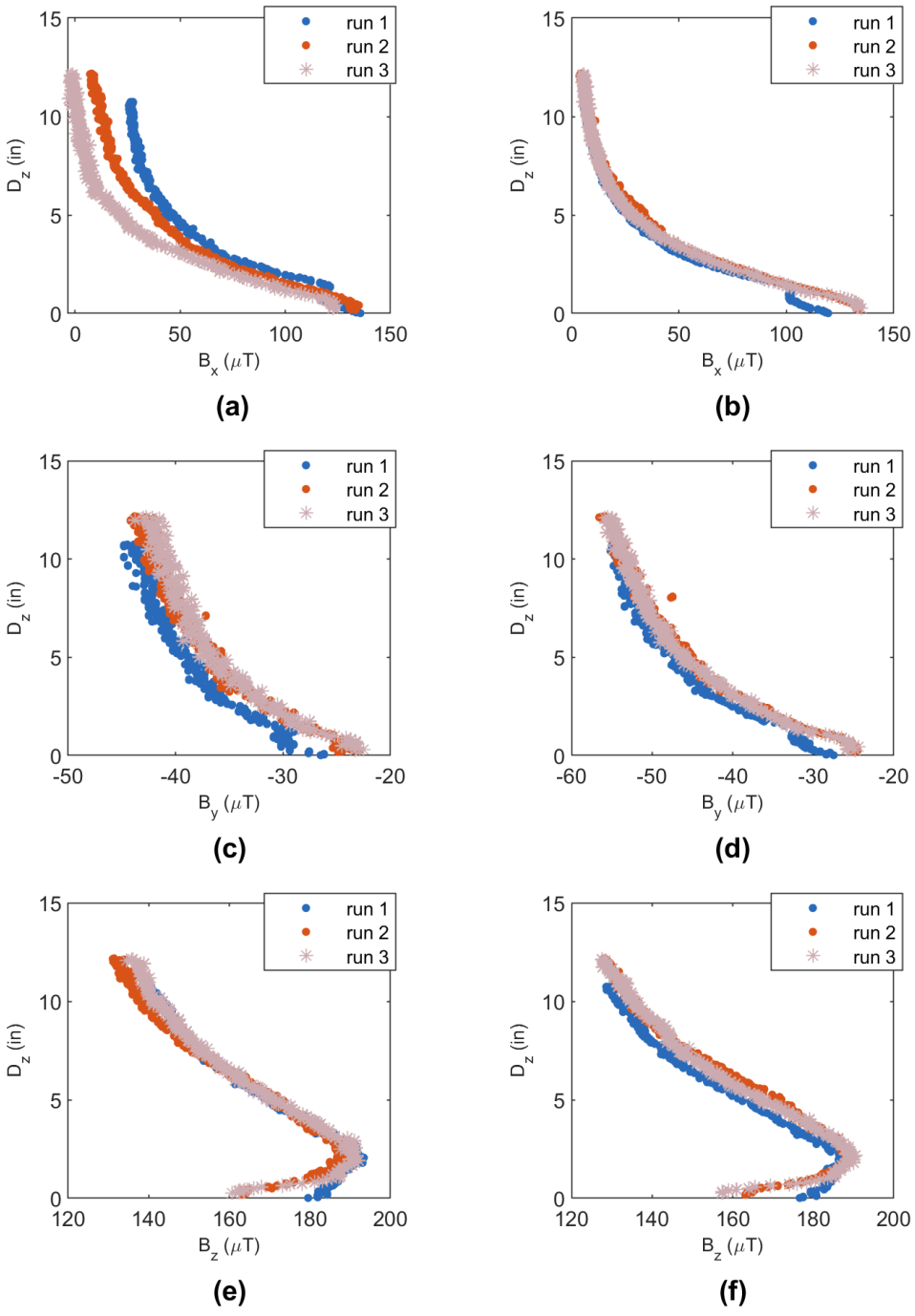

Figure 16. 3-DOF Raw Magnetic Anomaly Data as Measured by BNO055 and LIS3MDL in Vertical Motion Testing . (a), (c), (e) Magnetic anomaly measured by BNO055 in X, Y, and Z axes, respectively. (b), (d), (f) Magnetic anomaly measured by LIS3MDL in X, Y, and Z axes, respectively.

The average raw magnetic field strength data from the vertical motion scenario tests are shown in Fig. 17. To create a simple algorithm for determining the vertical distance from the first sensor to the pipe, the portions of the curve that could most closely embody a linear relationship were examined. The magnetic field strength measured from the z-axis of the sensors was found to be sufficiently linear for distances between 2 in and 10 in from the pipe. The following linear models were formulated according to this result:

$$D_z(B_{az}, B_{aT}) = \begin{cases} -0.1531B_{az} + 31.26 & if \quad 120 < B_{az} < 200\ \mu\text{T} \quad (6) \\ -0.1269B_{aT} - 28.41 & otherwise \quad (7) \end{cases}$$

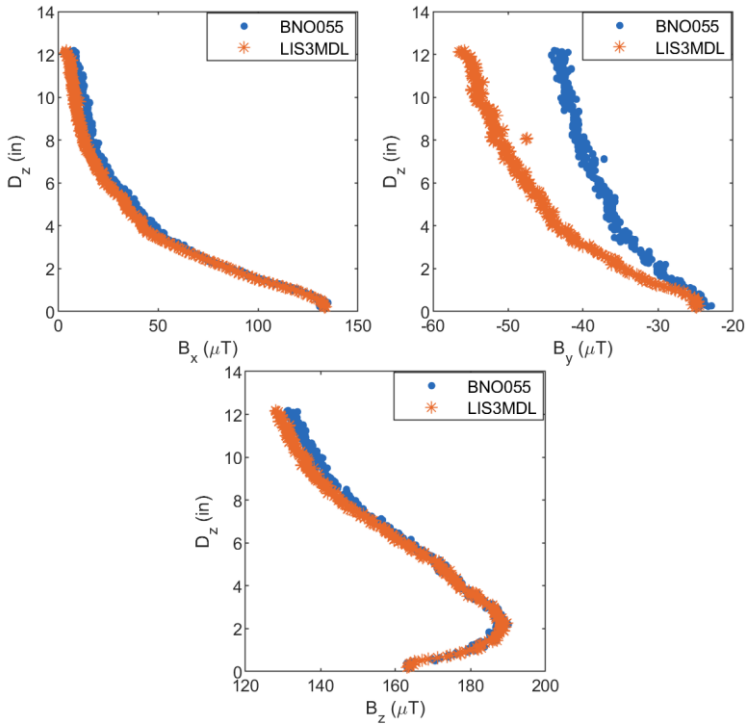

Figure 17. Average 3-DOF Magnetic Anomaly in Vertical Motion Testing

The algorithm shown in Figure 18 was developed to reflect the pipeline depth relative to the sensor in the real-time system. The algorithm generally relies on the anomaly measured along the axis of motion, or the z-axis. However, like the horizontal motion scenario, the total anomaly model could be used when the magnetic field strength is higher or when the sensor is closest to the pipe section.

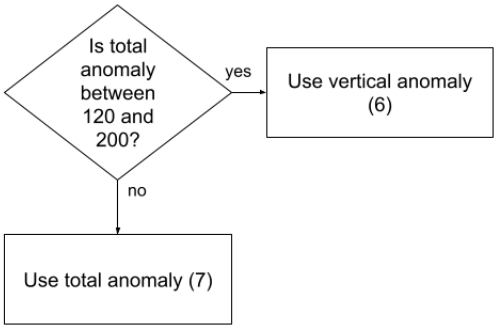

Figure 18. Vertical Depth Estimation Algorithm

3.3. Distance Estimation Results

Applying the models given in section 3.2 to the estimation algorithm, the result shown in Figure 19 was achieved. A comparison of the performances for both sensors is also shown. The BNO055 executed more consistent measurements during the data collection runs and thus produced better estimation results. The performance of the LIS3MDL may be a consequence of its high sensitivity, where small deviations in movement have a large impact on the reading.

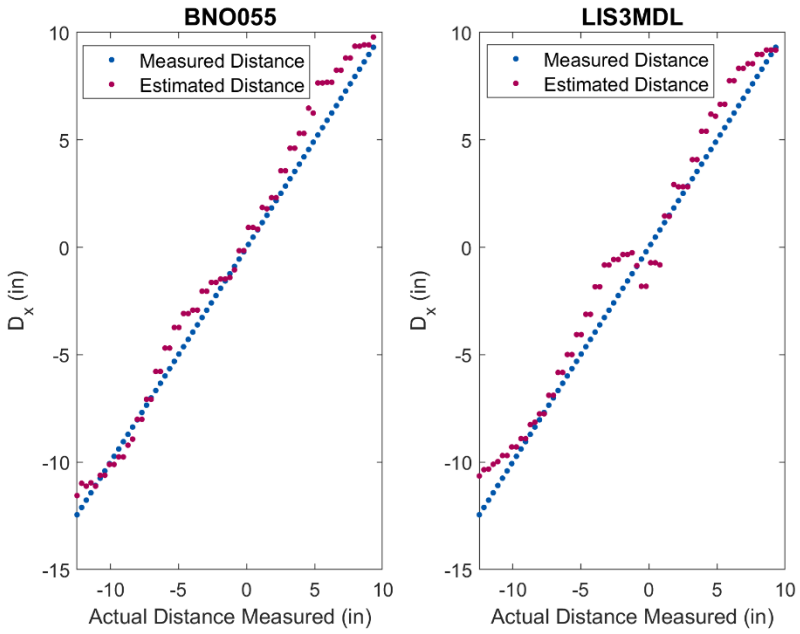

Figure 19. Horizontal Distance Estimation Result

Applying the linear models, (6) and (7) to the vertical depth estimation algorithm, yielded the results shown in Figure 20. This result confirms that the linear model used to estimate the distance when the sensor is 2-10 in from the pipeline is sufficient for determining the relative proximity of the excavator to the pipeline and consequently prevent dangerous collisions.

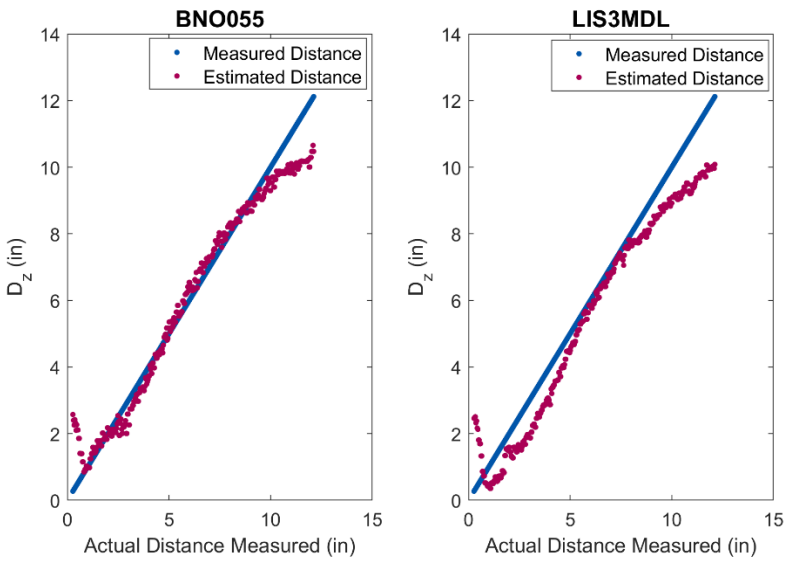

Figure 20. Vertical Distance Estimation Result

The error for each trial was calculated according to the percent variance from the reference measurement from the ultrasonic sensor. The average error and standard deviation associated with distance ranges for the horizontal motion and vertical motion scenarios are shown in Table 4 and Table 5, respectively. The error was higher for the 0 – 3 in distance range for both motion scenarios and sensors. This error can be attributed in part to the error contributed by the ultrasonic sensor in the reference distance measurements. The variations in measurements less than 2 in from the pipe section also impact the ability of the algorithm to correctly calculate the distance. To improve the error in the horizontal proximity tests, it may be necessary to account for the deviations in straight-line trajectory. The errors presented in Table 5 suggest that the method, when employing the BNO055 sensor, can accurately estimate distances between 3 and 9 inches. In the case of excavator digging, this is sufficient to prevent the bucket from colliding with a buried pipeline.

Table 4. Estimation Error of BNO055 and LIS3MDL in Horizontal Motion Trial

	BNO055		**LIS3MDL**	
Range (in)	Error (%)	Std	Error (%)	Std
9 – 6	6.14	3.91	7.07	4.72
6 – 3	8.94	7.01	14.7	5.65
3 – 0	19.9	11.4	17.6	13.4
0 – (-3)	15.5	10.7	45.3	27.6
(-3) – (-6)	10.9	6.70	17.3	12.5
(-6) – (-9)	13.5	4.40	4.14	2.95

Table 5. Estimation Error of BNO055 and LIS3MDL in Vertical Motion Trial

	BNO055		**LIS3MDL**	
Range (in)	Error (%)	Std	Error (%)	Std
9 – 6	3.04	1.98	4.71	2.73
6 – 3	5.17	3.52	13.8	9.12
3 – 0	11.4	7.76	39.9	13.3

Although the current performance of the system suggests the system can be used as a supplementary aid to prevent excavator buckets from colliding with pipeline, all potential sources of error should be addressed along with solutions to the errors. In the experiments described in the present work, the exact speed and heading of the model excavator could not be replicated across trials, thus the measurement data varies from trial-to-trail. Three runs were performed to reduce this variance; however, it may be necessary to average the data from more experimental runs. This would obtain proximity models that are more representative of the slight deviations in speed and heading of the excavator and therefore more robust for distance estimation. The sampling rate of the wireless sensor system may also be a limiting factor in the accuracy of the method. For the horizontal motion experiments, the excavator traveled across the box in about 12 seconds, and with a sampling rate of 5 Hz, the total number of data points for each trial was around 60. With a higher sampling rate, more data points can be collected and used to generate more accurate proximity models.

In addition to the sources of error in a lab setting, there are a handful of potential sources of error present in a real-world experiment. Heavy metal contamination in the soil due to pollution presents a challenge in distinguishing buried pipeline from a strong ferromagnetic contaminate. The presence of other objects that generate a magnetic field, such as power cables, also have the potential to distort the measurement data. There are several challenges to implementing the system in the current stage of development. First, the sensors must be oriented perpendicular to the pipe section to reveal the same characteristic curve outlined in this paper. Approaching the pipe from different angles would result in different curve shapes and thus would require different proximity models. Possible future studies to address these issues are described in the following section.

4. CONCLUSIONS

4.1. Conclusions

Using the MAD method, two sensors can effectively remove the geomagnetic background and measure the anomaly created by a steel pipeline when mounted to an excavator. This paper showed that the pipeline magnetic field strength characteristics can then be exploited to identify sensor location relative to pipeline by applying linear models in real-time. For distances between 3 – 9 in, the algorithm estimated the distance between the sensor and pipeline with up to 14% error for the horizontal motion scenario and up to 5% for the vertical motion scenario. The horizontal and vertical anomalies are also not strongly affected by random movement, thus offering good reliability for the excavation scenario. This paper also demonstrated the use of two different magnetic sensors for distance estimation and the comparative results.

Table 6 provides a comparison of the results achieved by the proposed method to other experiments employing magnetic anomaly inversion. Vo *et al*. scanned vertically and inverted the magnetic field strength to calculate the depth of a 6-in diameter steel pipe. This method produced accurate results and was verified through field trials, however, the measurement system only experienced stable motion and was not mounted to excavation equipment. Wu and Guo developed a robust inversion algorithm that attempted to estimate the depth of an iron pipeline along with several pipeline parameters such as pipeline length, outer diameter, azimuth, etc. Synthetic magnetic field data was fed to the algorithm and the depth was inverted at 10 different depths. The average error for each corresponding depth range is low and acceptable for engineering applications. This study only lacks inversions for much smaller distances along with

real-world development and implementation of the algorithm. Considering these works, the results achieved by the method described in this paper are promising. Although the distance estimation accuracy is lower in comparison, the current work realized real-time proximity estimation that is suitable for avoiding excavator collisions with underground pipeline.

Table 6. Comparison of Proposed Method to Relevant Literature

Author	**Application**	**Motion**	**Depth range (mm)**	**Error (%)**
Vo *et al* [25]	Integrity Management	Vertical	100 – 300	<2
			300 – 400	2.50
			400 – 500	3.40
Wu and Guo [26]	Integrity Management	Vertical	500 – 2000	~2
			2000 – 3500	~3.32
			3500 – 5000	~2.7
Lopez	Excavation	Vertical	0 – 80	11.4
			80 – 160	5.17
			160 – 240	3.04

4.2. Future work

The methods presented in this paper are exclusive to horizontal and vertical movement individually. In typical excavation construction scenarios, however, the bucket moves both forward and downward simultaneously. Thus, it is suggested that the method is tested when the trajectory of the bucket is circular. Additionally, the magnetic field strength of a pipe is largely determined by the material and diameter of the pipe. For pipes of smaller diameter, especially when buried deep below the surface, the signal will be weaker. Modeling should then be performed for pipes of different material and diameter in future studies. In the experiments described in this paper, the pipe section and measurement system were fixed according to the direction of magnetic north, thus the orientation of the pipeline was known. In a real-world implementation, the pipeline orientation will be unknown. Methods for determining the pipeline orientation should thus be explored and included in the algorithm. Furthermore, the excavator bucket was removed from the small-scale excavator to mount the sensors, however the intended location of the sensors on a full-scall excavator would be on the excavator bucket. The sensor placed at the tip of the excavator bucket would be used to measure the anomalous field while another sensor would be mounted at a fixed distance for reference. Finally, increasing the number of sensors in the system may help to improve the estimation accuracy.

REFERENCES

[1] US DOT Pipeline and Hazardous Materials Safety Administration, “All Reported Incident Cause Breakdown: 5 Year Average (2017-2021),” 2022. [Online]. Available: https://portal.phmsa.dot.gov/analytics/saw.dll?Portalpages&PortalPath=%2Fshared%2FPDM%20Public%20Website%2F_portal%2FSC%20Incident%20Trend&Page=All%20Reported

[2] S. Asadollahi Dolatabad, A. G. Doree, L. L. olde Scholtenhuis, and F. Vahdatikhaki, “Review of Detection and Monitoring Systems for Buried High Pressure Pipelines: Final Report,” University of Twente, Enschede, Netherlands, 2017. [Online]. Available: https://ris.utwente.nl/ws/portalfiles/portal/13483195/Final_Report_VELIN_I_M.pdf

[3] B. Yektakhah, J. Chiu, F. Alsallum and K. Sarabandi, "Low-Profile, Low-Frequency, UWB Antenna for Imaging of Deeply Buried Targets," *IEEE Geoscience and Remote Sensing Letters*, vol. 17, no. 7, pp. 1168-1172, July 2020, doi: 10.1109/LGRS.2019.2942007.

[4] J. Li, T. Guo, H. Leung, H. Xu, L. Liu, B. Wang, and Y. Liu, “Locating Underground Pipe Using Wideband Chaotic Ground Penetrating Radar,” *Sensors*, vol. 19, no. 13, pp. 2913. July 2019, doi:10.3390/s19132913.

[5] J. Lester and L.E. Bernold, “Innovative process to characterize buried utilities using Ground Penetrating Radar,” *Automation in Construction*, vol. 16, no. 4, pp. 546-555, July 2007, doi:10.1016/j.autcon.2006.09.004.

[6] M. I. A. Jalil, N. Sahriman, R. Ghazali, M. A. S. Iberahim, A. R. A. Rasam, and M. H. Razali, "Ground Penetrating Radar for Detecting Underground Pipe Buried in Different Type Materials," in *2019 IEEE 10th Control and System Graduate Research Colloquium (ICSGRC)*, 2019, pp. 156-161, doi: 10.1109/ICSGRC.2019.8837098.

[7] P. Gamba and S. Lossani, "Neural detection of pipe signatures in ground penetrating radar images," *IEEE Transactions on Geoscience and Remote Sensing*, vol. 38, no. 2, pp. 790-797, March 2000, doi: 10.1109/36.842008.

[8] F. Yang, X. Qiao, Y. Zhang, and X. Xu, "Prediction method of underground pipeline based on hyperbolic asymptote of GPR image," in *Proceedings of the 15th International Conference on Ground Penetrating Radar*, 2014, pp. 674-678, doi: 10.1109/ICGPR.2014.6970511.

[9] G. Terrasse, J. Nicolas, E. Trouvé, and É. Drouet, "Automatic localization of gas pipes from GPR imagery," in *2016 24th European Signal Processing Conference (EUSIPCO)*, 2016, pp. 2395-2399, doi: 10.1109/EUSIPCO.2016.7760678.

[10] X. Zhou, H. Chen, and T. Hao, "Efficient Detection of Buried Plastic Pipes by Combining GPR and Electric Field Methods," *IEEE Transactions on Geoscience and Remote Sensing*, vol. 57, no. 6, pp. 3967-3979, June 2019, doi: 10.1109/TGRS.2018.2889248.

[11] H. Liu, X. Huang, F. Han, J. Cui, B. F. Spencer, and X. Xie, "Hybrid Polarimetric GPR Calibration and Elongated Object Orientation Estimation," *IEEE Journal of Selected Topics in Applied Earth Observations and Remote Sensing*, vol. 12, no. 7, pp. 2080-2087, July 2019, doi: 10.1109/JSTARS.2019.2912339.

[12] X. Zhou, H. Chen, and J. Li, "Probabilistic Mixture Model for Mapping the Underground Pipes," *ACM Transactions on Knowledge Discovery from Data (TKDD)*, vol. 13, no. 5, pp. 1-26, 2019, doi:10.1145/3344721.

[13] M. N. Zahari, S.W. Wahab, A. Madun, S.A. Khan, S.H. Dahlan, and M.N. Isa, "Detection and Characterization of Buried Objects Using Seismic Reflection Technique," in *FIG Congress 2018*, Instanbul, Turkey, 2018. [Online]. Available: https://www.fig.net/resources/proceedings/fig_proceedings/fig2018/papers/ts02f/TS02F_wahab_zahari_et_al_9481.pdf

[14] J. Dai and D. Xu, "Detection of underground pipeline based on Golay waveform design," in *AIP Conference Proceedings*, vol. 1864, no. 1, August 2017, doi: 10.1063/1.4992968.

[15] B. Handlon, S. J. Lorenc, L. Bernold, and G. Lee, "Tool integrated electromagnetic pulse induction technology to locate buried utilities," in *2000 IEEE International Symposium on Circuits and Systems (ISCAS)*, 2000, pp. 529-532, vol. 2, doi: 10.1109/ISCAS.2000.856382.

[16] B. T. Kolera, and L. E. Bernold, "Intelligent utility locating tool for excavators," *Journal of construction engineering and management*, vol. 132, no. 9, pp. 919-927, 2006, doi: 10.1061/(ASCE)0733-9364(2006)132:9(919).

[17] D. Liu, Y. Zhang, Z. Xia, Z. Zhao, T. Zhang, Y. Yang, and H. Shi, "Localization Estimation of Magnetic Targets Using Airborne Magnetic Anomaly Detection," in *2021 IEEE 4th International Conference on Electronics Technology (ICET)*, 2021, pp. 701-705, doi: 10.1109/ICET51757.2021.9451092.

[18] A. Sheinker, L. Frumkis, B. Ginzburg, N. Salomonski, and B. Kaplan, "Magnetic Anomaly Detection Using a Three-Axis Magnetometer," *IEEE Transactions on Magnetics*, vol. 45, no. 1, pp. 160-167, Jan. 2009, doi: 10.1109/TMAG.2008.2006635.

[19] B. Ginzburg, L. Frumkis, and B. Kaplan, "Processing of magnetic scalar gradiometer signals using orthonormalized functions," *Sensors and Actuators A: Physical*, vol. 102, no. 1-2, pp. 67-75, 2002. [Online]. Available: https://www.academia.edu/27836253/Processing_of_magnetic_scalar_gradiometer_signals_using_orthonormalized_functions

[20] H. Jin, J. Guo, H. Wang, Z. Zhuang, J. Qin, and T. Wang, "Magnetic Anomaly Detection and Localization Using Orthogonal Basis of Magnetic Tensor Contraction," *IEEE Transactions on Geoscience and Remote Sensing*, vol. 58, no. 8, pp. 5944-5954, Aug. 2020, doi:10.1109/TGRS.2020.2973322.

[21] A. Sheinker and M. B. Moldwin, “Magnetic anomaly detection (MAD) of ferromagnetic pipelines using principal component analysis (PCA),” *Measurement Science and Technology*, vol. 27, no. 4, March 2016, doi:10.1088/0957-0233/27/4/045104.

[22] D. Zhao, Z. Guo, J. Du, Z. Liu, W. Xu, and G. Liu, “Geometric modeling of underground ferromagnetic pipelines for magnetic dipole reconstruction-based magnetic anomaly detection,” *Petroleum*, vol. 6, no. 2, 2020, doi:10.1016/j.petlm.2019.06.001.

[23] Q. Pan, D. Liu, Z. Guo, H. Fang, and M. Feng, “Magnetic anomaly inversion using magnetic dipole reconstruction based on the pipeline section segmentation method,” *Journal of Geophysics and Engineering*, vol. 13, no. 3, pp. 242-258, June 2016, doi:10.1088/1742-2132/13/3/242.

[24] S. Feng, D. Liu, X. Cheng, H. Fang, and C. Li, “A new segmentation strategy for processing magnetic anomaly detection data of shallow depth ferromagnetic pipeline,” *Journal of Applied Geophysics*, vol. 139, pp. 65-72, April 2017, doi:10.1016/j.jappgeo.2017.02.009.

[25] C. K. Vo, D. M. J Cowell, C. Cookson, S. Freear, S.G.H. Staples, and B.T.H. Varcoe, “Determining the Depth and Location of Buried Pipeline by Magnetometer Survey,” *Journal of Pipeline Systems Engineering and Practice*, vol. 11, no. 2, 2020, doi:10.1061/(ASCE)PS.1949-1204.0000438.

[26] P. Wu and Z. Guo, “High-Precision Inversion of Buried Depth in Urban Underground Iron Pipelines Based on AM-PSO Algorithm for Magnetic Anomaly,” *Progress in Electromagnetics Research C*, vol. 100, pp. 17-30, Jan. 2020, doi:10.2528/PIERC19110701.

[27] L. Chen, Y. Feng, P. Wu, W. Zhu and G. Fang, "An Innovative Magnetic Anomaly Detection Algorithm Based on Signal Modulation," *IEEE Transactions on Magnetics*, vol. 56, no. 9, pp. 1-9, Sept. 2020, Art no. 6200609, doi: 10.1109/TMAG.2020.3005896.

[28] Bosch Sensortec, “BNO055 Intelligent 9-axis absolute orientation sensor,” BNO055 datasheet, Nov. 2014.

[29] STMicroelectronics, “Digital output magnetic sensor: ultra-low-power, high-performance 3-axis magnetometer,” LIS3MDL datasheet, May 2017.